



# Growth of III-nitrides on Si(1 1 1) by molecular beam epitaxy Doping, optical, and electrical properties

E. Calleja<sup>a,\*</sup>, M.A. Sánchez-García<sup>a</sup>, F.J. Sánchez<sup>a</sup>, F. Calle<sup>a</sup>, F.B. Naranjo<sup>a</sup>,  
E. Muñoz<sup>a</sup>, S.I. Molina<sup>b</sup>, A.M. Sánchez<sup>b</sup>, F.J. Pacheco<sup>b</sup>, R. García<sup>b</sup>

<sup>a</sup>Dpt. Ing. Electrónica, ETSI Telecomunicación, Universidad Politécnica, Ciudad Universitaria, 28040 Madrid, Spain

<sup>b</sup>Dpt. Ciencia de Materiales e Ingeniería Metalúrgica y Química Inorgánica, Universidad de Cádiz, Apdo. 40, 11510 Puerto Real, Cádiz, Spain

---

## Abstract

The growth of high-quality III-nitrides by plasma-assisted molecular beam epitaxy on Si(1 1 1) substrates is addressed. A combination of optimized AlN buffer layers and a two-step growth process leads to GaN layers of high crystal quality (8 arcmin X-ray diffraction full-width at half-maximum) and flat surfaces (57 Å rms). Low-temperature luminescence spectra, dominated by excitonic emissions at  $3.465 \pm 0.002$  eV, reveal the presence of a biaxial tensile strain of thermal origin. AlGa<sub>x</sub>N layers, grown within the alloy range  $0.10 < x < 0.76$ , have flat surfaces and exhibit strong excitonic luminescence. Si-doping of GaN and AlGa<sub>x</sub>N produces n-type films reaching electron densities up to  $2 \times 10^{19}$  and  $8 \times 10^{19}$  cm<sup>-3</sup>, respectively. From photoluminescence and Hall data analysis a Si-donor ionization energy between 50 and 60 meV is derived in GaN. The exciton bound to Si neutral donors at 3.445 eV redshifts while the *c*-axis lattice parameter decreases as the Si-doping increases, indicating an enhancement of the biaxial tensile strain in the film. This strain increase is a consequence of a strong reduction of the density of dislocations reaching the free surface, due to a particular grain size and orientation governed by the presence of Si donors. Be-doping is also achieved on GaN giving the shallowest acceptor activation energy reported so far, around 90–100 meV. However, there is a severe limitation of the Be incorporation on substitutional sites, leading to the formation of complex, deep defects. © 1999 Elsevier Science B.V. All rights reserved.

**Keywords:** Molecular beam epitaxy; Photoluminescence; Crystal morphology; Doping effects; MOVPE

---

## 1. Introduction

Group III-nitrides are being largely exploited for commercial fabrication of blue light emitting diodes (LED) and room temperature cw operating laser diodes (LD) with lifetimes over 8000 h [1].

Although the main advances relate to nitrides grown on substrates like sapphire and SiC by metal organic vapour-phase epitaxy (MOVPE), the growth of wurtzite III-nitrides by molecular beam epitaxy (MBE) on Si(1 1 1) is quite appealing due to the doping capability, crystal quality, thermal stability, and potential integration offered by these unexpensive substrates. The quality of III-nitrides grown on Si(1 1 1) using electron cyclotron resonance (ECR) [2,3], or radio frequency (RF) [4]

---

\* Corresponding author. Tel.: +34-1-336-7315/7322; fax: +34-1-336-7323; e-mail: calleja@die.upm.es.

nitrogen plasma sources, or by direct decomposition of ammonia on the substrate [5], has been significantly improved in the past few years. The high quality of the III-nitrides grown on Si(1 1 1) is backed by the achievement of devices like field-effect transistors [6], Schottky-barrier ultraviolet detectors [7], and blue LEDs [8].

This work will review the main achievements on the Ga(Al)N growth by MBE on Si(1 1 1) substrates as well as on the optical, transport, and doping properties. Crystal morphology is assessed by atomic force microscopy (AFM), scanning, and transmission electron microscopy (SEM, TEM). Crystallinity and mosaicity is characterized by X-ray diffraction (XRD), TEM, and high-resolution electron microscopy (HREM). Transport and optical properties in undoped and doped (Si, Be) Ga(Al)N are analyzed by Hall effect and secondary ion mass spectroscopy (SIMS), and by low-temperature continuous-wave and time-resolved photoluminescence (PL).

## 2. Growth optimization of AlN buffers on Si(1 1 1)

The growth of wurtzite III-nitrides on Si(1 1 1) substrates follows a standard cleaning procedure by a modified RCA method. The substrates are then mounted on In-free molybdenum holders, loaded into the MBE system and outgassed at 850°C–900°C for 30 min to remove the native oxide. A  $1 \times 1$  RHEED reconstruction with prominent Kikuchi lines is then observed, that turns into a  $7 \times 7$  reconstruction at 750°C, typical of clean Si(1 1 1) surfaces. The nitrogen is generally provided by pure ammonia or by a plasma source, in our case, a RF Oxford CARS25 with an optical-detector system that allows to keep the amount of active nitrogen constant. More details about the system setup are given in Ref. [4].

When a GaN layer is grown directly on the cleaned Si(1 1 1) surface, a thin amorphous layer develops in between, most probably  $\text{Si}_x\text{N}_y$ , generated by reaction of the Si surface with the active nitrogen. The formation of such amorphous layers was reported by Ohtani et al. [2] and by Stevens et al. [9]. Fig. 1 shows that above the amorphous

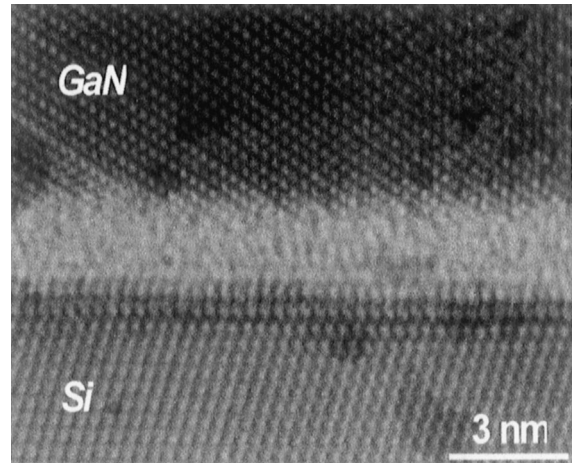
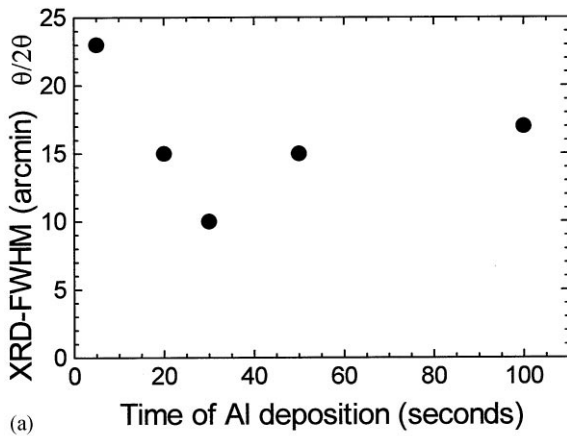


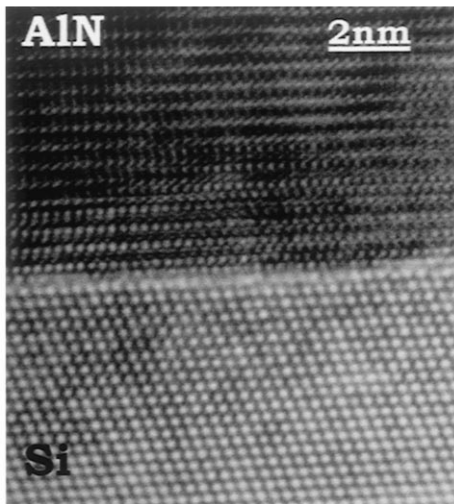
Fig. 1. HRTEM micrograph showing the development of an amorphous, thin (20–30 Å)  $\text{Si}_x\text{N}_y$  layer at the GaN/Si(1 1 1) interface.

layer the GaN grows keeping a crystalline structure, but the result is a polycrystal with FWHM values from XRD measurements between 70 and 100 arcmin. A way to avoid this amorphous layer formation is to start the growth with an AlN buffer layer, because the bond formation between Al and N atoms prevails over the Si–N one. Simultaneously, the AlN buffer layer strongly favours the subsequent growth of the GaN layer, because there is a match between atomic planes of Si and AlN following a 4 : 5 ratio [6]. Very nice results showing abrupt interfaces between the AlN layer and the Si(1 1 1) substrate have been obtained by MBE using an ECR plasma source [3]. Another method to prevent an amorphous layer formation is to deposit a few Al monolayers on the clean Si surface before turning the plasma source on, then, an AlN buffer layer is grown. The effect of the Al monolayers, grown epitaxially on Si(1 1 1) [11], was checked on a GaN layer grown on top giving best XRD-FWHM values of 10 arcmin and a root mean-square (rms) surface roughness of 13 nm [10] (Fig. 2a). Following this procedure very sharp AlN/Si(1 1 1) interfaces are achieved (Fig. 2b).

In addition to an AlN high crystal quality, a very flat surface is required in order to achieve a two-dimensional (2D) GaN growth, since steps and



(a)



(b)

Fig. 2. (a)  $\theta$ - $2\theta$  XRD-FWHM of GaN layers grown on AlN-buffered Si(1 1 1) as a function of the Al coverage. (b) HRTEM micrograph of a sharp and clean AlN/Si(1 1 1) interface.

terraces are found to promote inversion domain boundaries [12–14] and to develop cubic GaN inclusions embedded into the hexagonal matrix [15–18]. These cubic inclusions are present in AlN (Fig. 3), but in all cases these cubic inclusions remain near the interface and do not reach the free surface. In some cases, a rotation of the AlN planes driven by substrate steps has been reported [3,19]. These rotated grains may contribute to the generation of threading dislocations that propagate into the upper layers.

In order to optimize the AlN buffer layer, the growth temperature and stoichiometry have to be

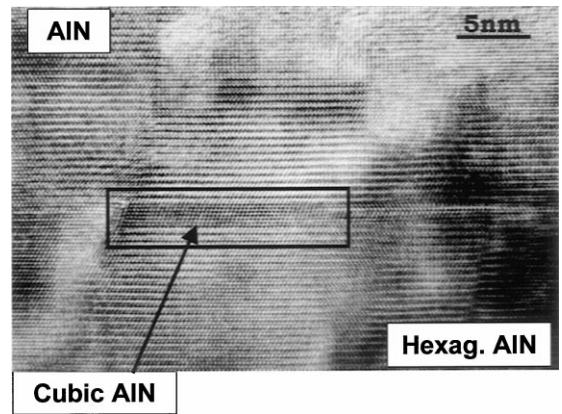


Fig. 3. HRTEM micrograph indicating the presence of cubic inclusions embedded in the hexagonal matrix for AlN layers.

carefully considered. Fig. 4 represents the AlN growth rate as a function of the Al flux (beam equivalent pressure, BEP) for three different amounts of active nitrogen [4,20]. A common feature is the saturation of the growth rate at a given Al flux, that defines a stoichiometric condition. Below this point the growth proceeds under N-rich conditions and above it there is an Al-rich regime that may eventually lead to Al droplets formation. When the growth takes place near stoichiometry, optimum AlN buffers are obtained in terms of surface flatness (Fig. 5) and crystal quality (Fig. 6) at growth temperatures around 850°C [20]. Lower growth temperatures lead to an increasing surface roughness and to polycrystals [21]. This is a quite different approach as that generally followed in MOVPE-grown AlN buffers, that are first deposited at rather low temperatures (< 500°C) and then recrystallized at a much higher temperature (above 1000°C). The main result from Fig. 6 (10 arcmin XRD-FWHM) has to be compared with previous reports by Stevens et al. [9] (26 arcmin), by Meng et al. [22] (51 arcmin), and recently by Yasutake et al. [23] (55 arcmin), that used the same approach of Al coverage prior to the AlN buffer growth. It is worth to mention that XRD spectra in Fig. 5 were obtained from  $\theta/2\theta$  scans with a wide open detector, that give very close FWHM values as those derived from rocking curve scans [20].

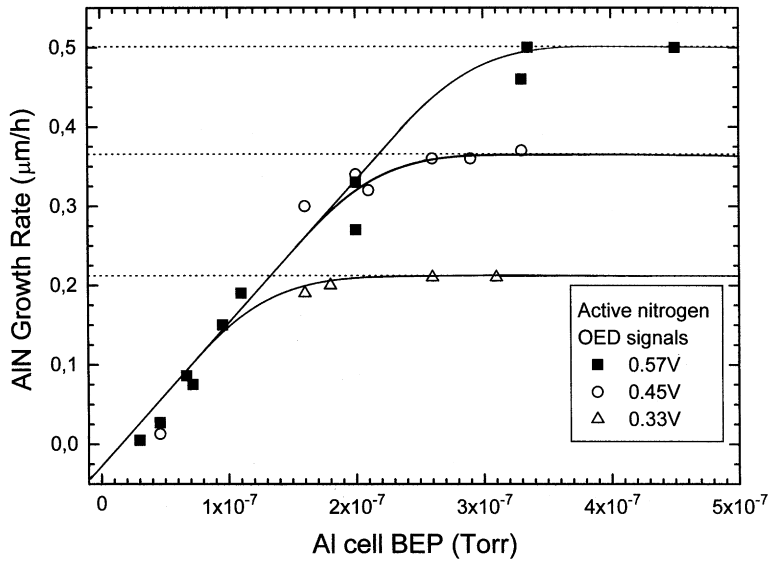


Fig. 4. AIN growth rate as a function of the Al flux (BEP) for three different amounts of active nitrogen. Solid lines are guides to the eye.

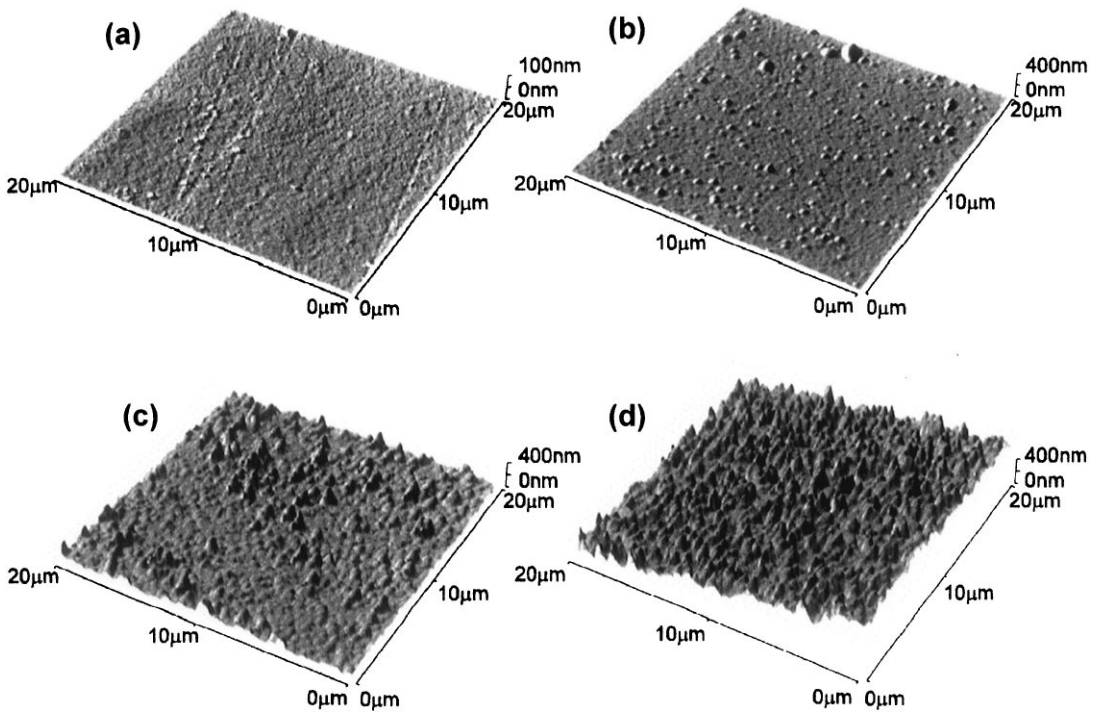


Fig. 5. AFM surface roughness evolution (rms) of AIN layers as a function of the Al flux. (a) 7.6 nm (slightly above stoichiometry); (b) 8.5 nm (near stoichiometry); (c) 44 nm (low N-rich conditions) and (d) 79 nm (high N-rich conditions).

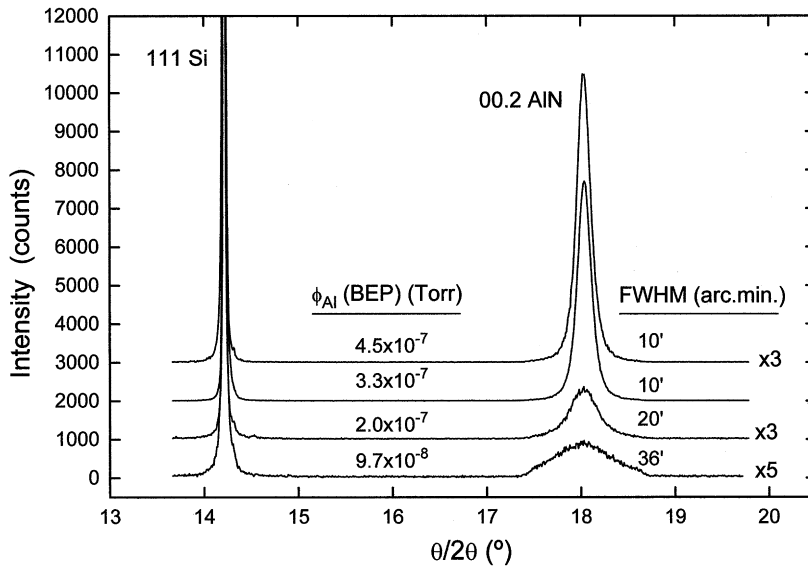


Fig. 6. High-resolution XRD spectra from AlN layers grown at different Al fluxes for a given amount of active nitrogen. Open detector configuration.

### 3. Growth optimization of GaN on AlN buffered Si(1 1 1)

High-quality GaN layers are grown on optimized AlN buffers on Si(1 1 1) for specific growth conditions. Fig. 7 shows the GaN growth rate versus the Ga flux for temperatures between 660°C and 770°C and a given amount of active nitrogen [4,33]. Unlike the AlN case, raising the growth temperature needs a higher Ga flux to reach the same growth rate, indicating that a substantial Ga desorption takes place at the surface. An estimation of the activation energy of this desorption process gives 2.2 eV, in very good agreement with data by Guha et al. [24]. A steep increase of the Ga desorption rate was found earlier for growth temperatures above 700°C by Powell et al. [25] and Yu et al. [26] in GaN grown by MBE on sapphire substrates.

Depending on the effective III–V ratio, taking into account the Ga-desorption rate, the morphology of the GaN layers changes dramatically. N-rich conditions lead to highly columnar, whisker-like morphologies (Fig. 8) where the columns are aligned along the (0 0 0 1) direction having an average diameter of 60 nm and a height that depends only on the growth time/rate [4]. Similar results are

obtained independently of the buffer layer and substrate used (Fig. 8), but always under N-rich conditions. Yoshizawa et al. [27] report columnar GaN grown by RF-MBE on sapphire where, apparently, this morphology appears under a Ga-rich regime, but the growth takes place at 800°C at which there must be a huge Ga desorption. The columnar structure has already been reported to be typical, under given growth conditions, of highly mismatched systems [28], and the driving mechanisms seem to be related to the Ga adatom diffusion that is strongly reduced under N-rich conditions [29]. Early reports on columnar growth were given by Gaskill et al. [30] in GaN grown by MOVPE using hydrazine as nitrogen source.

When the growth proceeds at stoichiometry or Ga-rich conditions the GaN layer becomes compact, as it is shown in Fig. 9a. Changes in morphology as a function of the III/V ratio are reproducible, and mixed GaN layers, first compact and then columnar can be grown starting at stoichiometry and following with a steep reduction of the Ga-flux. The density of columns depends on how far this second growth step lies from stoichiometry (Fig. 9b and Fig. 9c). Notice that the column height depends only on the growth time/rate.

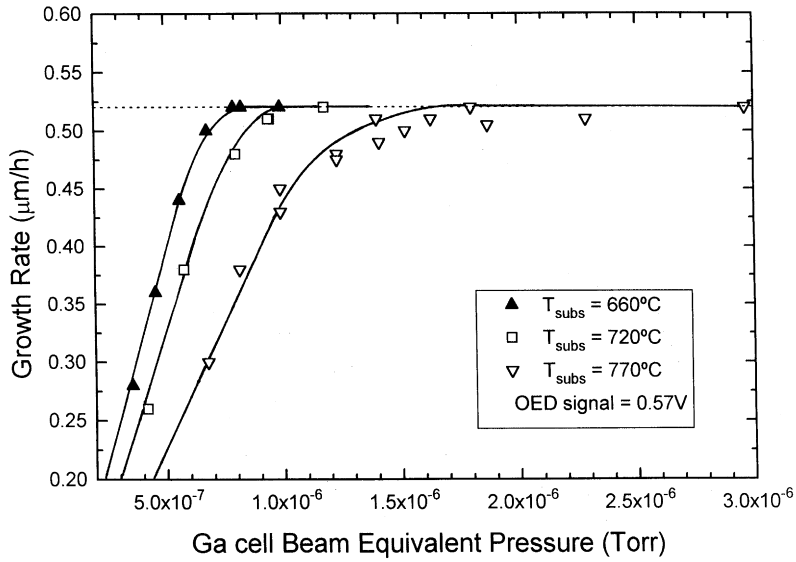


Fig. 7. GaN growth rate as a function of the Ga flux (BEP) for three different substrate temperatures and a given amount of active nitrogen. Solid lines are guides to the eye.

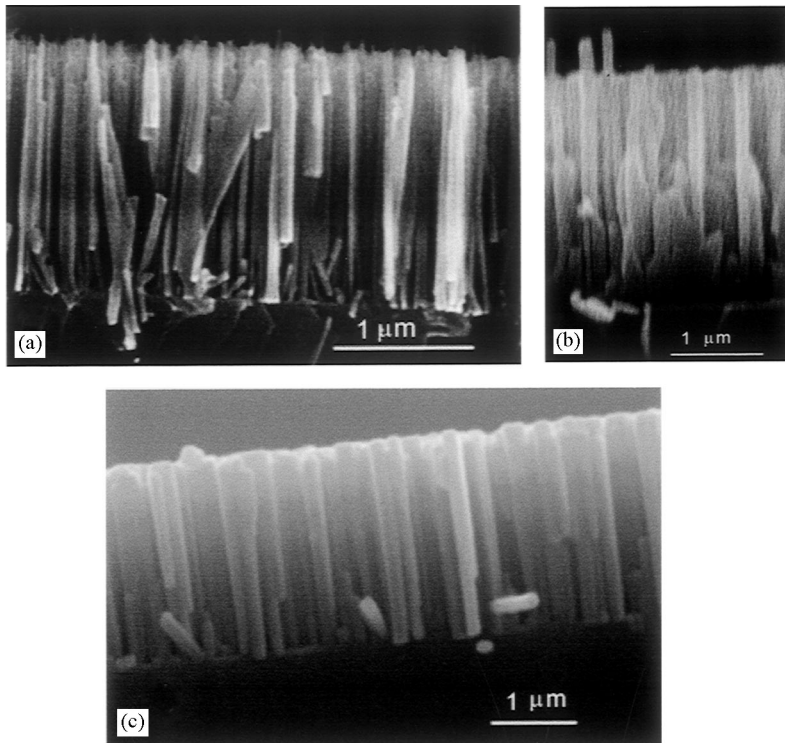


Fig. 8. Cross-sectional SEM micrographs of GaN layers grown by MBE under N-rich conditions: (a) directly on Si(1 1 1); (b) on AlN-buffered Si(1 1 1) and (c) on  $\text{Al}_2\text{O}_3$ .

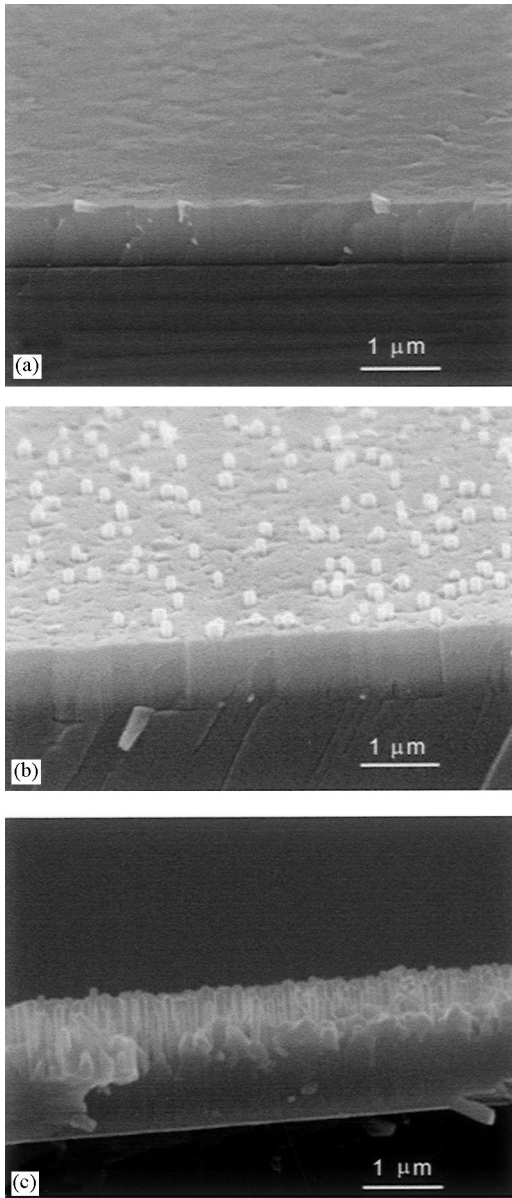


Fig. 9. Morphology of GaN layers as a function of the III/V ratio as observed by SEM photographs: (a) under slightly Ga-rich conditions or at stoichiometry; (b) and (c) mixed GaN layers, first compact and then columnar with increasing column density as the III/V ratio becomes more N-rich.

It is worth to mention that columnar GaN layers are fully relaxed from lattice and thermal strain, having a very high crystal quality characterized by strong and narrow excitonic PL [31]. However, the

columnar structure may restrain or even inhibit parallel conduction due to potential barriers (grain boundaries) and/or physical isolation between columns. This point will be considered in Section 5, where the transport properties are addressed.

A further improvement in crystal morphology and quality can be achieved following a two-step growth method [10]: an initial GaN growth at slow rate by pulsing the Ga shutter, that promotes the coalescence of 3D islands, then, a second step at a nominal rate of  $0.5 \mu\text{m/h}$ . Fig. 10 shows the evolution of RHEED pattern, that reveals a clear  $\times 2$  reconstruction during the GaN layer growth [55]. By means of an optimized AlN buffer and the two-step GaN growth mode, a surface roughness of 6 nm (rms); XRD-FWHM values of 8 arcmin; very strong and narrow (15 meV) excitonic low-temperature PL; residual n-type concentrations of  $2 \times 10^{17} \text{cm}^{-3}$ ; and the absence of yellow luminescence have been recently reported [10,32,33]. The crystal quality improvement is clearly observed in Fig. 11a and Fig. 11b in terms of XRD-FWHM values and low-temperature PL spectra. Previous results on GaN layers reported XRD-FWHM values of 22 arcmin by Ohtani et al. [2], 36 arcmin by Meng et al. [22], and 50 arcmin by Kung et al. [34]. PL spectra in Fig. 11b have best line widths of 15 meV, as compared to previous values of 23 and 20 meV by Ohtani et al. [2] and Godlewski et al. [5], respectively. Hellman et al. [35] report on GaN layers grown on optimized AlN buffers deposited in a different way, starting at  $500^\circ\text{C}$ , then, raising steeply the temperature to the optimal value, slightly below the RHEED  $7 \times 7$  to  $1 \times 1$  transition ( $830^\circ\text{C}$ ). GaN layers grown on top of optimized AlN buffers, following the different procedures described [10,35] have flat surfaces slightly undulated and dislocation densities in the mid- $10^9 \text{cm}^{-2}$  range (Fig. 12a and Fig. 12b). However, the GaN surface becomes much rougher when a non-optimized growth leads to a higher dislocation density. It is worth mentioning that in such cases the “V”-shaped profiles are related to threading dislocations (Fig. 12c) in a way that reminds the surface striation in metamorphic InGaAs/GaAs heterostructures [36]. Optimized GaN layers show a  $\times 2$  reconstruction (Fig. 10), a rather flat surface (Fig. 12a and Fig. 12b), and a very small wet etching rate,

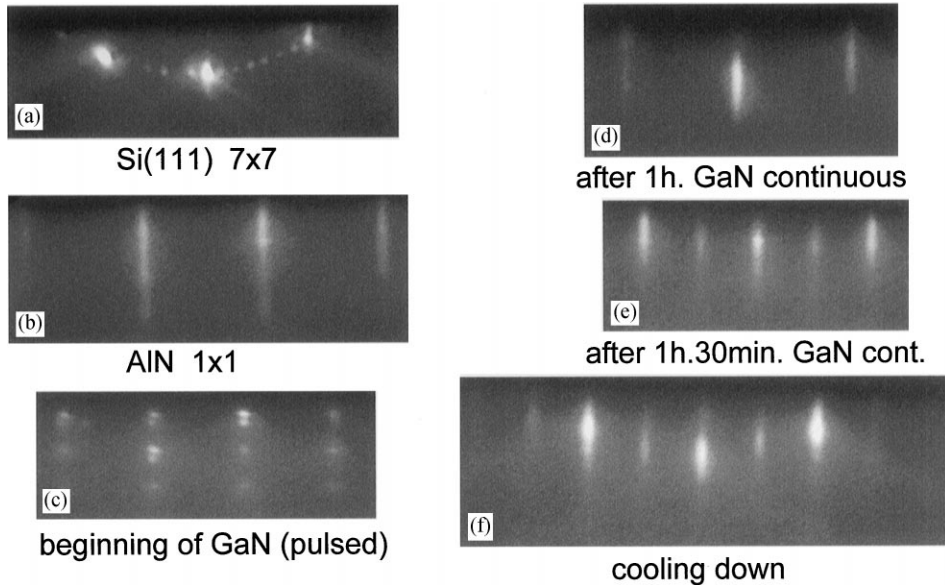


Fig. 10. RHEED pattern evolution during the growth of optimized GaN/AlN/Si(1 1 1) structures. (a)  $7 \times 7$  reconstruction of the clean Si(1 1 1) substrate; (b)  $1 \times 1$  reconstruction of the AlN buffer layer; (c) through (e) different stages of GaN growth and (f) during the cooling down stage. A  $2 \times 2$  reconstruction is clearly observed after approximately 1 h of growth and during the cooling process.

all of them being features associated to Ga-terminated surfaces[37,38].

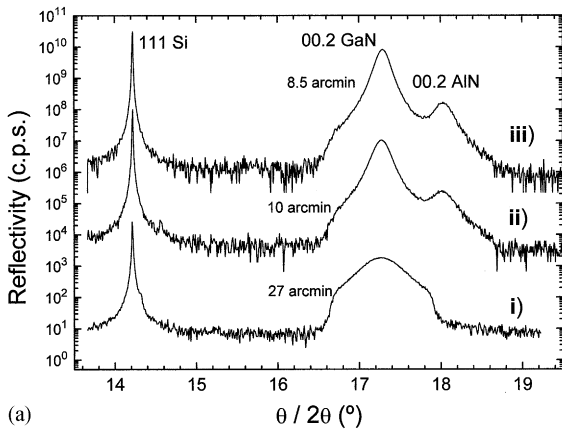
Different approaches have been tried to grow high-quality GaN layers on Si substrates. Yang et al. [39] reported 25 arcmin XRD-FWHM values using a strained AlN/GaN superlattice buffer. GaN was grown on thin SiC layers obtained by carbonization of a silicon-on-insulator (SOI) [39,40] substrate. Nitridation of composite substrates like (1 1 1)GaAs/Si was used to grow AlN/GaN(In) heterostructures with strong room temperature PL [41]. GaN has also been grown on Si substrates with an intermediate thin aluminum oxide layer (“compliant” substrates), either deposited by LPCVD [42] or converted from AlN by selective oxidation [43]. Results from these approaches are in general far from the state of the art.

#### 4. Growth of AlGaN layers on AlN buffered Si(1 1 1)

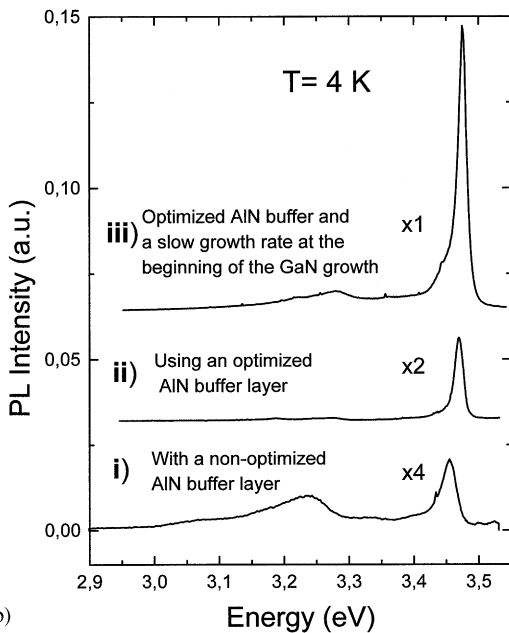
High-quality AlGaN layers have been grown at  $770^\circ\text{C}$  on optimized AlN buffers, with Al contents

ranging from 10% to 76%. The Al mole fraction follows a linear relationship with the Al flux (BEP) as shown in Fig. 13. A sharp  $\times 2$  surface reconstruction is observed along the growth, characteristic of a 2D growth mode, leading to smooth surface morphologies that do not degrade with increasing Al mole fraction, as it is seen in Fig. 14. XTEM imaging shows a very smooth surface for a 11% AlGaIn layer (Fig. 15). As in the case of GaN, cubic grains embedded in the hexagonal matrix were found located near the AlGaIn/AlN interface, but not reaching the free surface. A high density of planar defects that stop at the grain boundaries was also observed. Best surface roughness values from AFM measurements give  $33 \text{ \AA}$  (rms).

Fig. 16 shows a typical low-temperature PL spectrum of an AlGaIn layer with dominant excitonic emissions, that follow the bandgap dependence with the Al mole fraction assuming the bowing factor given by Brunner et al. [44,45]. Notice that there is no presence of the yellow band. There is a controversy regarding the bandgap dependence with the Al mole fraction, that some authors reported to follow a linear relationship in thick



(a)



(b)

Fig. 11. (a) High-resolution XRD spectra of GaN layers after different optimization processes: (i) grown on top of a non-optimized AlN buffer; (ii) using an optimized AlN buffer, and (iii) using an optimized AlN buffer layer and a two-step GaN growth mode (see text). (b) Low-temperature PL spectra corresponding to the samples in (a).

AlGaN layers grown on sapphire [46,47], whereas in other cases it was found to bow downwards [48–50]. More recently, a downwards bowing has been measured in AlGaN samples covering the whole composition range, either grown on sapphire by MBE [44,45] or on 6H-SiC by MOVPE [51],

using different techniques to precisely determine the Al composition. Similar results were reported by Huang et al. [52] in AlGaN grown on sapphire by pulsed laser deposition. On the other hand, a linear relationship was determined for a smaller Al mole fraction range ( $0 < x < 0.3$ ) in AlGaN grown on sapphire by MBE [53] and by MOVPE [54], although in the later case the AlGaN was grown on top of a 2  $\mu\text{m}$  thick GaN layer. When AlGaN layers are under thermal strain, a simple XRD measurement of the  $c$ -axis lattice constant may underestimate (compressive strain) or overestimate (tensile strain) the Al mole fraction, as it is the case of the AlGaN layers shown in Fig. 16b. Assuming biaxial tensile strain values in AlGaN (for  $x < 0.3$ ) similar to those found in GaN layers grown on Si(1 1 1) [55], the relative shift in  $c$ -axis lattice parameter due to the strain is about 0.03%. On the other hand, from the linear dependence between the  $c$ -axis lattice parameter and the Al% [52,53], a 0.04% change in  $c$  corresponds roughly to 1% Al. Accordingly, data in Fig. 16b should be shifted to 1% lower Al mole fractions, but the bowing factor is not significantly affected.

FWHM values from XRD data in AlGaN/AlN/Si(1 1 1) layers are between 16 and 22 arcmin for all Al mole fractions considered, being higher than those of GaN layers. These values are halfway between those reported by Huang et al. [52] in AlGaN/Al<sub>2</sub>O<sub>3</sub> grown by pulsed laser deposition (25–30 arcmin) and by Angerer et al. [44,45] by MBE (15 arcmin), but much higher than those given by Li et al. [56] (2 arcmin) in AlGaN grown by gas-source MBE on top of 2  $\mu\text{m}$  thick GaN layers. The AlGaN growth temperature in the referred works was between 800°C and 1000°C, and better results are expected for AlGaN on Si(1 1 1) substrates raising the temperature from 770°C and adjusting the III/V ratio because, as it was found for AlN buffers (Fig. 4), a growth close to stoichiometric conditions leads to smoother surfaces. It is worth mentioning that, because of their smooth surfaces, AlGaN layers were used as buffers to grow GaN on top, and preliminary results show a significant improvement of the GaN surface morphology as compared to the best results discussed in Section 3.

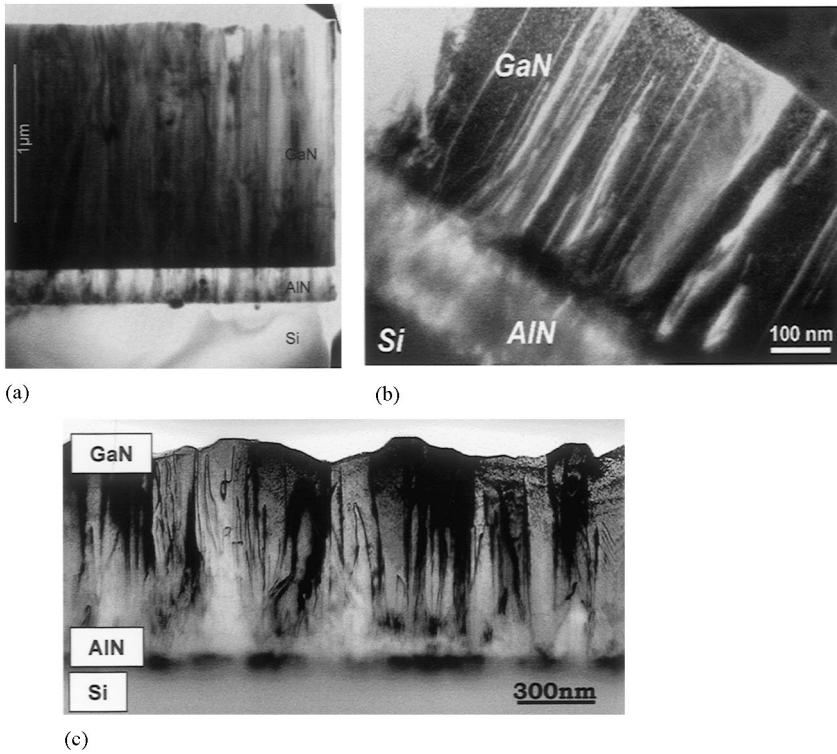


Fig. 12. HRTEM micrographs of GaN/AIN/Si(1 1 1) samples: (a) from Ref. [35]; (b) GaN layer grown on optimized AlN buffer, and (c) nonoptimized growth (see text).

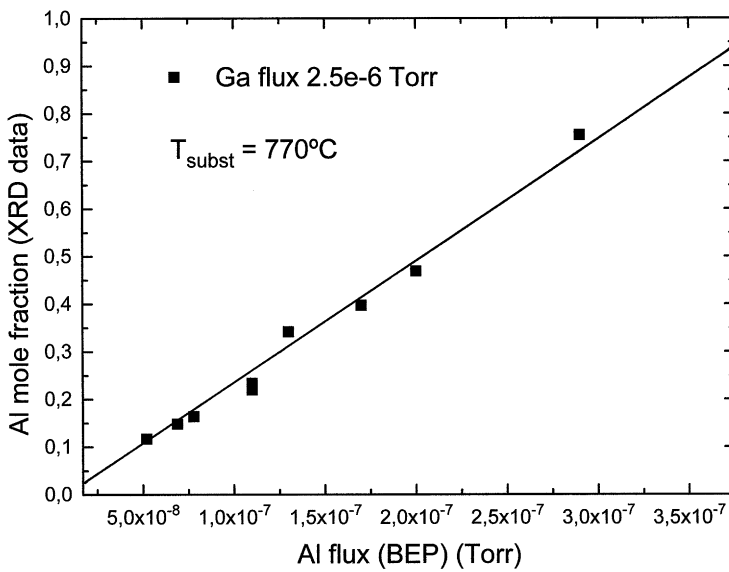


Fig. 13. Al mole fraction (from XRD data) dependence on the Al flux for a given Ga flux.

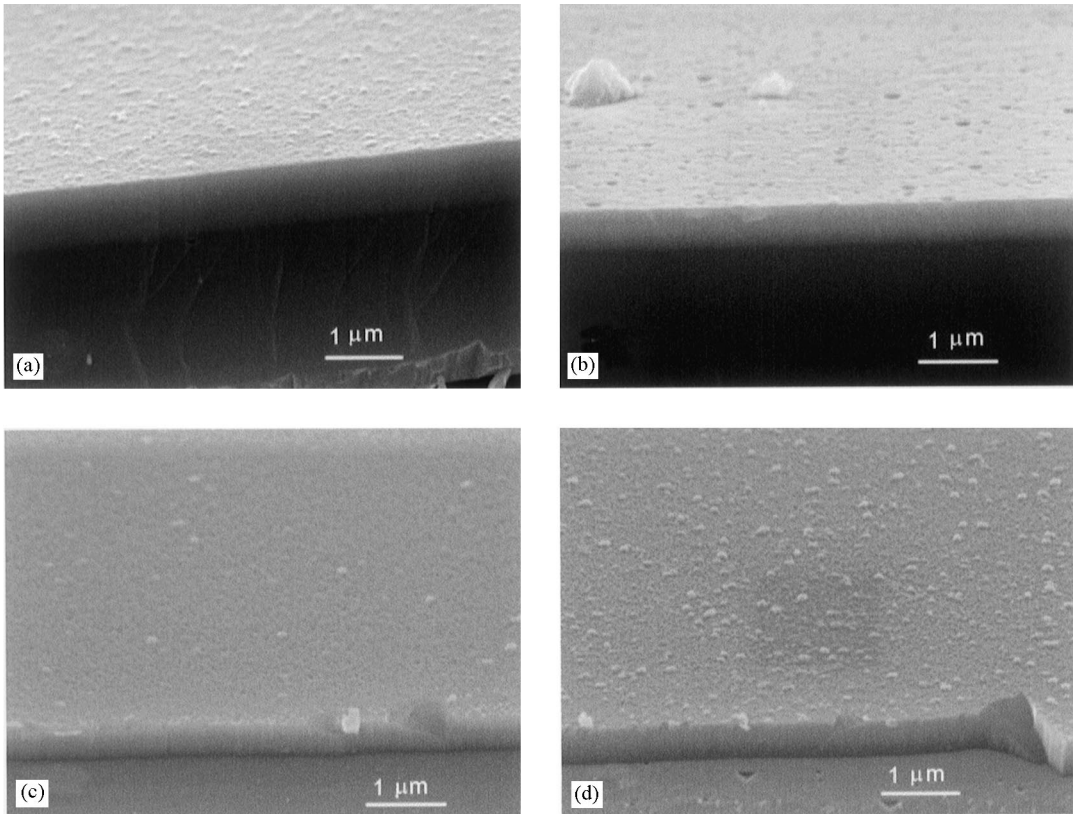


Fig. 14. SEM micrographs of AlGaIn layers with different Al compositions: (a) 11%; (b) 14%; (c) 46%; and (d) 76%.

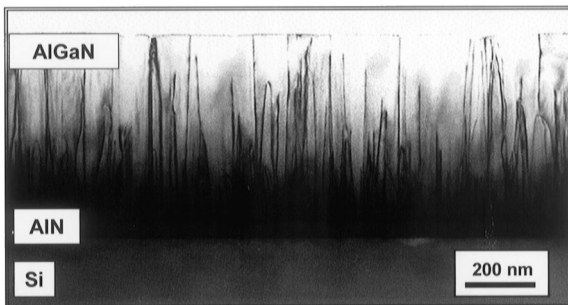


Fig. 15. XTEM image of an  $\text{Al}_{11}\text{Ga}_{89}\text{N}$  layer grown on an AlN-buffered Si(1 1 1) substrate.

## 5. Transport properties in undoped GaN layers

As it was shown in Fig. 7, the saturation of the GaN growth rate versus Ga flux determines the

stoichiometry point that delimits two distinct growth modes, N-rich and Ga-rich leading to quite different crystal morphologies (Section 3). Room temperature Hall measurements were first performed in undoped samples *without* AlN buffers [33], and the carrier concentration, conductivity type, and mobility values are shown in Fig. 17. Samples grown at  $660^\circ\text{C}$  have an n-type conductivity strongly dependent on the Ga flux. Sharp electron density changes, driven by an increasing N flux from conductive to semi-insulating, were already reported in MBE-grown GaN/ $\text{Al}_2\text{O}_3$  [57,58]. In our case, the low conductivity found in samples grown at  $660^\circ\text{C}$  under low Ga flux (N-rich) may be due to the columnar morphology typical for these growth conditions [33] (Fig. 8). The very high electron densities reached in samples grown at  $660^\circ\text{C}$  under Ga-rich conditions cannot be

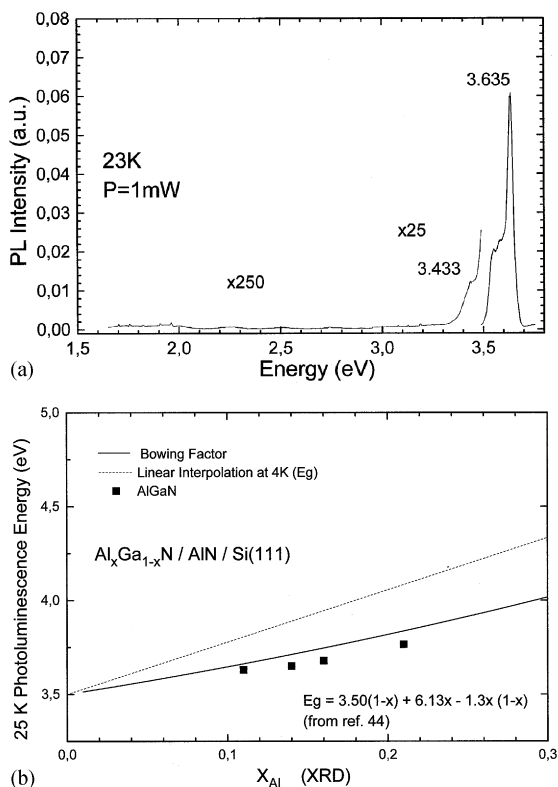


Fig. 16. (a) Low-temperature PL spectrum of an  $\text{Al}_{11}\text{Ga}_{89}\text{N}$  layer; (b) Low-temperature PL emission dependence on Al% determined by XRD.

accounted for by contamination (O, Si, C), but most likely by native defects. Indeed, samples subjected to a rapid thermal annealing (RTA) under a  $\text{N}_2$  atmosphere show no electron density increase, whereas a clear enhancement is observed when the RTA is performed under an Ar atmosphere (Fig. 18). These results point to native defects, most likely  $\text{V}_\text{N}$ , as the most probable origin of the residual n-type conductivity.

Samples grown at higher temperatures ( $> 700^\circ\text{C}$ ) show an apparent p-type conductivity with no dependence on the growth regime, either N-rich or Ga-rich (Fig. 17a). This apparent p-type conductivity has no relation with the GaN layer, but with a parallel conduction path through a highly conductive p-type channel at the GaN/Si(1 1 1) interface generated by a Ga/Si interdiffusion process, since Ga is a shallow acceptor in Si. SIMS

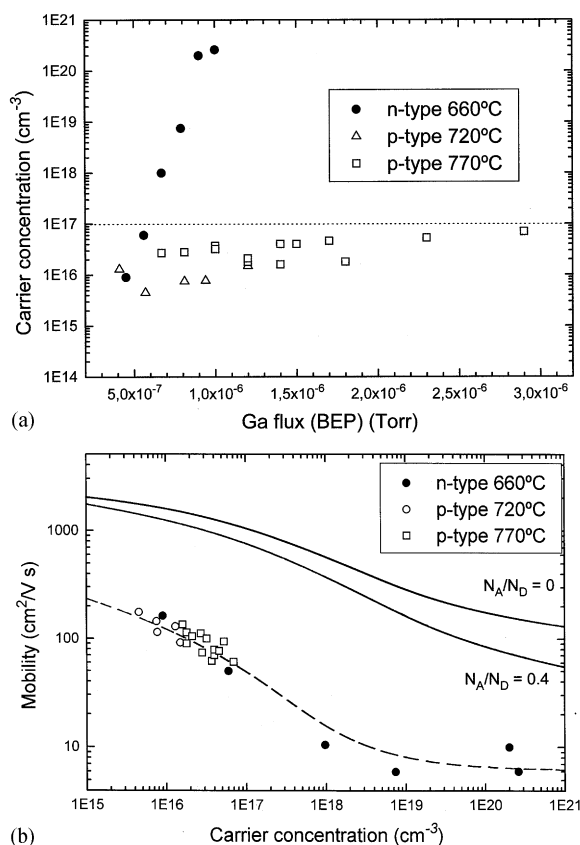


Fig. 17. (a) Room-temperature Hall-carrier density versus Ga flux for undoped GaN layers grown without AlN buffer. (b) Room-temperature Hall mobility versus carrier density for undoped GaN layers in (a). Solid lines are theoretical fits with  $N_\text{A}/N_\text{D}$  compensation ratios of 0 and 0.4 after Ref. [58]. Dashed line is a guide to the eye.

measurements reveal this diffusion process with onset temperatures around  $600^\circ\text{C}$ , and temperature-dependent Hall measurements have determined the Ga and Al acceptor ionization energies in GaN/Si(1 1 1) and GaN/AlN/Si(1 1 1) respectively [33]. This diffusion process makes Hall data unreliable in most GaN samples, even grown on AlN buffered Si(1 1 1). In order to estimate the residual n-type conductivity in GaN samples grown above  $700^\circ\text{C}$ , Schottky barriers have been fabricated on top of the layers. From the slope of the reciprocal capacitance versus reverse voltage plot, a donor concentration around  $2 \times 10^{17} \text{ cm}^{-3}$

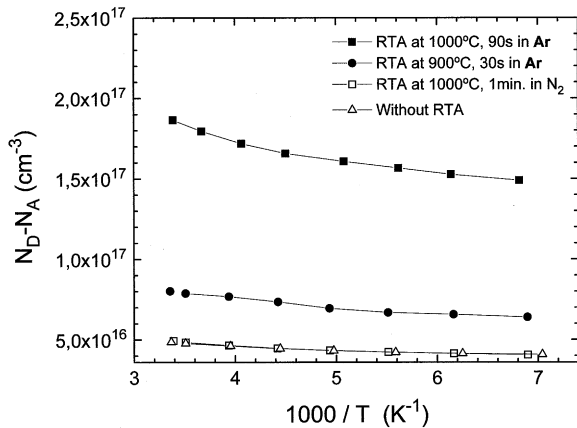


Fig. 18. Temperature dependence of the electron density for undoped n-type GaN layers after different rapid thermal annealing (RTA) processes.

is derived. The same value is obtained in samples where the Si(1 1 1) substrate and AlN buffer were previously removed by chemical etching.

The electron mobility values in Fig. 17b (samples grown at 660°C) follow qualitatively the theoretical model [59], but they are 10 times lower than those reported for GaN on sapphire [60,61]. Compensation alone cannot account for such low mobilities and a strong scattering process due to a high dislocation density must be present [62,63]. Indeed, these layers, grown *without* AlN buffer, were rather polycrystalline with XRD-FWHM values between 70 and 100 arcmin (Section 2). Mobility values derived from Hall measurements in optimized GaN layers on AlN buffers are unreliable because of the parallel conduction at the interface already mentioned.

## 6. Photoluminescence in undoped GaN layers

Optimized GaN layers grown as described in Section 3 display low-temperature PL spectra dominated by intense emissions from 3.463 to 3.467 eV with 15 meV line width (Fig. 19) and no yellow band is present. For a given sample, the energy position of the dominant peak does not shift with excitation power, showing no intensity saturation within a power range of 0.01–10 mW, and its

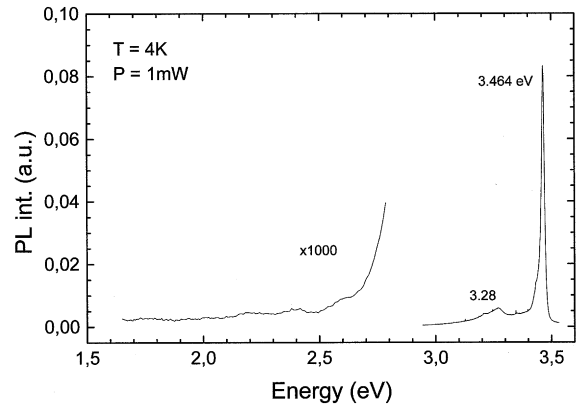


Fig. 19. Low temperature PL spectrum of an undoped GaN layer grown on AlN/Si(1 1 1).

temperature dependence fits accurately that of the bandgap, following the model by Fan [64]. Time-resolved PL spectra tuned at 3.464 eV have exponential decays with lifetimes of 150 ps which are similar to those observed for the free exciton A (FXA) at 3.478 eV and the DBE at 3.472 eV in relaxed, columnar GaN layers on Si(1 1 1) [31,33]. These results lead to conclude that the emission at  $3.465 \pm 0.002$  eV (Fig. 19) correspond to the FXA or DBE transitions in GaN under residual biaxial strain of thermal origin. The *c*-axis lattice parameter of these samples has been measured by XRD at room temperature, thus, the biaxial residual strain at low temperature is determined and related to the PL excitonic emission measured at 4 K. Taking the relaxed value of the *c*-axis lattice parameter ( $c_0$ ) equal to 5.1856 Å [65], the strain at low temperature can be expressed by a linear approximation as

$$\varepsilon_{zz}(T) = \varepsilon_{zz}(300)(1 + (300 - T)/(T_G - 300)), \quad (1)$$

with  $\varepsilon_{zz} = (c - c_0)/c_0$  and  $T_G$  the growth temperature. The PL emissions at  $3.465 \pm 0.002$  eV are very close to the FXA position (some 6–7 meV below) under biaxial tensile strain determined by Shikanai et al. [66] (Fig. 20a). This may indicate that, eventhough the intensity of this emission does not saturate with the excitation power in the range studied, it might relate to a DBE transition rather than to the FXA, although both transitions may be

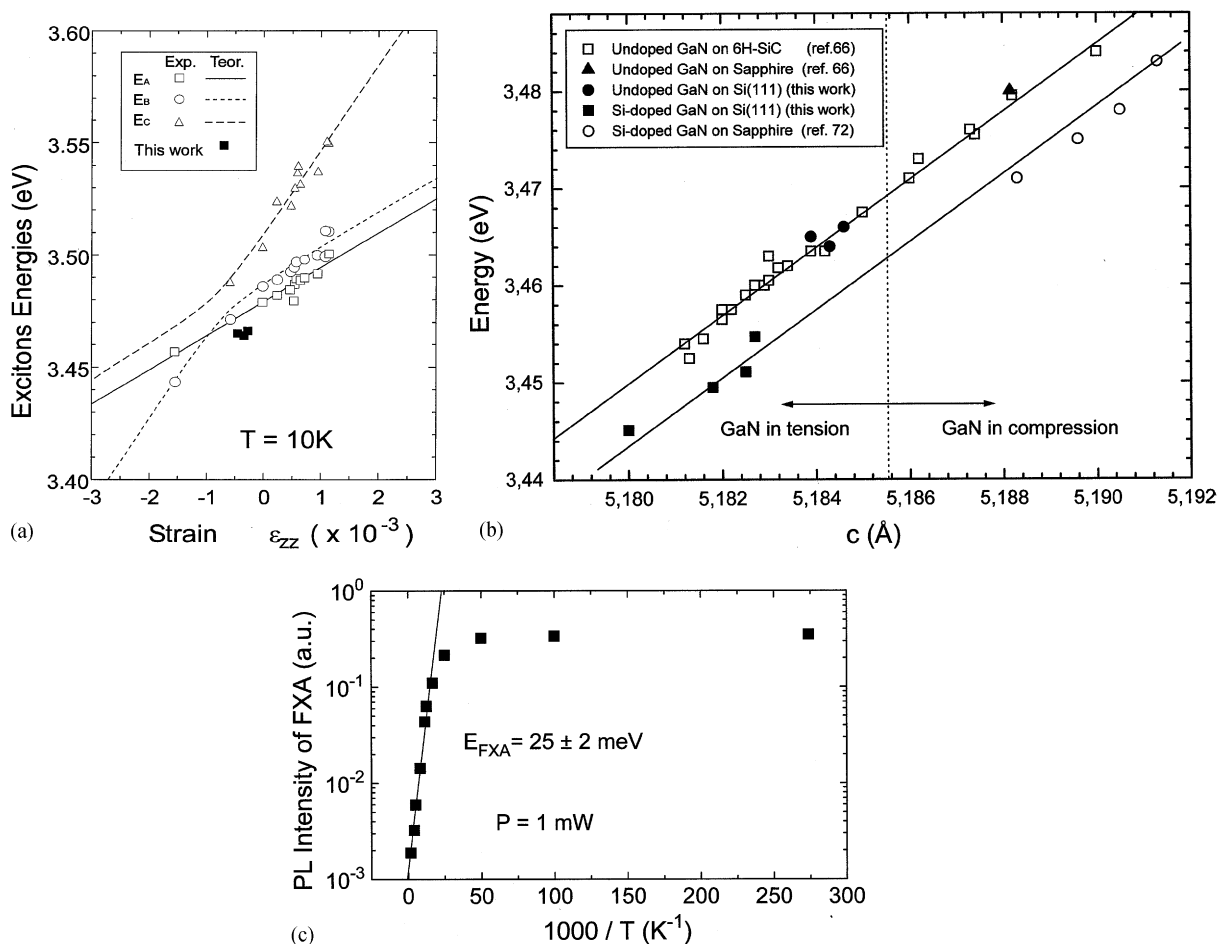


Fig. 20. (a) Low temperature excitonic PL emission energy dependence on the biaxial strain in undoped GaN layers grown on Si(1 1 1).  $E_A$ ,  $E_B$ , and  $E_C$  correspond to the free excitons A, B, and C respectively (Ref. [65]). (b) Low-temperature donor bound exciton emission energy, in undoped and Si-doped GaN layers grown on various substrates, versus  $c$ -axis lattice constant. (c) Binding energy derived from the thermal quenching of the FXA emission in an undoped, relaxed GaN layer grown on Si(1 1 1) (columnar morphology).

present within the 15 meV wide PL peak (Fig. 19). Further evidence is obtained from the correlation of the PL emission energies with the measured  $c$ -axis lattice parameter [67], that gives a very good fit when considering DBE transitions (Fig. 20b). For these undoped samples under biaxial tensile strain, the bandgap energy can be estimated from the PL band edge emissions, taking into account the binding energy of the FXA and the energy difference between the FXA and DBE transitions (6–7 meV). Since the strain does not modify the

heavy hole mass in GaN [66], we will consider the binding energy of the relaxed FXA measured from the thermal quenching of its intensity in an undoped, relaxed (columnar) GaN layer grown on Si(1 1 1) [31] that is  $25 \pm 2 \text{ meV}$  (Fig. 20c), in very good agreement with previous values of 26.1 meV [68,69] and 26.7 meV [70]. Then, depending on the nature assumed for the excitonic PL emissions at 3.465 eV (FXA or DBE), a bandgap energy between 3.491 and 3.497 eV is obtained.

## 7. Si-doped Ga(Al)N layers on AlN buffered Si(111)

Several Si-doped GaN layers, all 1  $\mu\text{m}$  thick, were grown at 760°C on Si(111) substrates, using 0.5  $\mu\text{m}$  thick, high-temperature (910°C) AlN buffers. Fig. 21a shows the low temperature PL spectra of these samples, where the dominant peak at around 3.45 eV redshifts while the *c*-axis lattice parameter decreases, as the Si-doping density increases. For Si-doping densities above  $5 \times 10^{18} \text{ cm}^{-3}$  the dominant PL peak blueshifts and broadens as a consequence of the band filling and potential fluctuations due to the random distribution of Si impurities [71–73]. Similar PL redshifts, reported in Si-doped GaN/Al<sub>2</sub>O<sub>3</sub> layers as a function of the Si-doping level, were interpreted in terms of compressive biaxial strain relaxation, either by generation of Si-related defects [74] or by a reduction and random distribution of the dislocation density [75], being both interpretations somehow discrepant. A band renormalization was proposed by Zhang et al. [76] to explain this redshift, neglecting changes of the compressive residual strain because of the nominally equal layer thicknesses. However, Fig. 21a shows that GaN layers with the same measured thickness (1  $\mu\text{m}$ ) do have different residual strain due to different Si-doping densities. Very recently, Oh et al. [71] suggested potential fluctuations by impurities or local defects, as well as hydrostatic strain due to atomic size differences between Si and Ga atoms as the main reasons for the PL redshift. However, the PL redshift in Fig. 23 is observed for Si-doping levels as low as  $1.7 \times 10^{17} \text{ cm}^{-3}$ , so that, lattice distortion by impurities or nonstoichiometric defects [77], hydrostatic strain by point defects [78], or lattice expansion by heavy Si doping [79] cannot be invoked, since in all cases densities above  $1 \times 10^{19} \text{ cm}^{-3}$  are required.

The PL redshift together with the *c*-axis lattice parameter reduction, observed in Fig. 21a as the Si-doping level increases, point to an enhancement of the biaxial tensile strain. This is in contrast with reports of similar PL redshifts observed in GaN/Al<sub>2</sub>O<sub>3</sub> layers, where the biaxial compressive strain is relaxed, either by the generation of point defects [74] or by a reduction of the threading

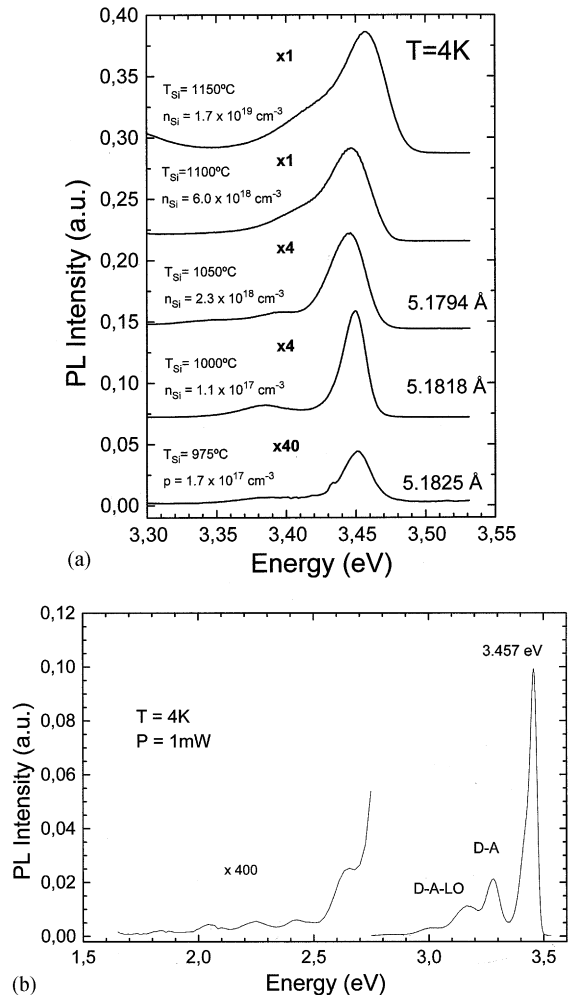


Fig. 21. (a) Low-temperature PL emissions of Si-doped GaN layers as a function of the Si-doping. The values of the *c*-axis lattice constant are derived from XRD data. (b) Low-temperature PL spectrum of a Si-doped GaN sample ( $n = 1.7 \times 10^{19} \text{ cm}^{-3}$ ). Notice that there is no yellow band present in the spectrum.

dislocations reaching the free surface [75]. Lee et al. [73] pointed out that a dislocation density reduction would increase the strain instead of relaxing it. However, a more homogeneous (random) distribution of a lower dislocation density may relax more efficiently the residual strain. The Si-doping would affect the dislocation structure, either by modifying the atom mobility and/or the number of growth islands during the initial GaN growth stages [75].

We have found a strong reduction in the density of threading dislocations for Si doping levels above  $1 \times 10^{18} \text{ cm}^{-3}$ , almost an order of magnitude as compared to undoped layers (from  $6 \times 10^9$ – $8 \times 10^8 \text{ cm}^{-2}$ ). This dislocation density reduction is due to a particular orientation and size of the crystal subgrains, namely, by an increase of the “out plane” (tilt) subgrain misorientation, together with an increase in the density of planar defects. A tilt increase will promote dislocations parallel to the growth plane. Both, the planar defects and the dislocations parallel to the interface will force the threading dislocations to bend by interaction, so that, a significant reduction of the dislocations reaching the free surface will occur [59,80].

The increase of the PL spectra intensity with the Si-doping and the main peak energy position difference, as compared to that of undoped GaN layers (Fig. 19), suggest that the dominant peak in Fig. 21a is related to Si-donors. Fig. 21b shows the PL spectrum of a Si-doped GaN sample ( $1.7 \times 10^{19} \text{ cm}^{-3}$  in Fig. 21a) where, besides the main peak related to Si-donors, a donor–acceptor pair (DAP) transition and its first phonon replica are observed, most probably involving carbon acceptors. Notice that there is no yellow band present in the spectrum. The main peak at 3.457 eV follows the bandgap temperature dependence and its intensity tends to saturate within a power range of 0.01–10 mW, but there is no energy shift, when increasing the excitation power density. In addition, time-resolved PL decays show exponential and fast slopes, similar to those corresponding to the DBE transition in relaxed, columnar GaN and undoped compact GaN layers [31,33] mentioned in Section 6. From these results we conclude that the main PL peak in Fig. 21b has a DBE character. Going back to Fig. 20b, and considering the energy difference between the DBE transitions involving residual donors and Si-donors, we can estimate a binding energy of the excitons bound to neutral Si-donors of 12–13 meV. Following the Hayne’s rule [81], a Si-donor ionization energy of 60–65 meV is derived. There are several reports on PL from Si-doped GaN that lead to similar energies. Data from Si-doped GaN/Al<sub>2</sub>O<sub>3</sub>, by Lee et al. [74], agree quite well with our results, as it is shown

in Fig. 20b. Wickenden et al. [82] found a binding energy of 8.6 meV for the exciton bound to Si-neutral donors in GaN/Al<sub>2</sub>O<sub>3</sub> that leads to a 43 meV ionization energy considering a factor of 5 generally assumed for donors [81]. Kawakami et al. [83] report a bound exciton with a binding energy of 11.6 meV assumed to involve acceptors, but taken as a DBE emission as proposed by Orton and Sakai [84], the Hayne’s rule [81] yields 58 meV for the donor ionization energy. In this case, the GaN layers were nominally undoped, but, as a matter of fact, Si is a common impurity in MOVPE and this possibility, although speculative, should not be openly disregarded. Results from temperature dependent Hall data in these layers and in Si-doped GaN/Al<sub>2</sub>O<sub>3</sub> grown by MOVPE, lead to Si-donor ionization energies about 50 meV, in good agreement with values derived from PL spectra analysis. A comparative analysis and discussion of the different values found in the literature for the Si-donor ionization energy are given in Ref. [55].

AlGaIn layers were also doped with silicon reaching electron concentrations up to  $8 \times 10^{19} \text{ cm}^{-3}$  for Al mole fractions up to 40% (a Si-cell temperature of 1150°C). Beyond this Al% value the doping efficiency drops sharply. For the same Si-cell temperature (1050°C) that generates an electron density of  $3 \times 10^{18} \text{ cm}^{-3}$  in GaN, AlGaIn layers with 46% Al have a much lower n-type conductivity, and increasing the Al mole fraction to 76% Al leads to semi-insulating material. Mobility values around  $15 \text{ cm}^2/\text{V s}$  were measured in samples with electron densities of  $8 \times 10^{19} \text{ cm}^{-3}$ , in good agreement with previous values reported in Si-doped AlGaIn grown on 6H-SiC [85] by MOVPE and on sapphire by pulsed laser deposition [52].

A decrease of the electron concentration in undoped AlGaIn layers has been reported by Kahn et al. [47] and by Lee et al. [86], leading to semi-insulating crystals beyond 60% Al mole fractions. Bremser et al. [51] reported a similar behavior in intentionally Si-doped AlGaIn layers for Al mole fractions higher than 42%, but later on, the same group reported on a Si-doped AlGaIn layer with 58 Al% where the Hall electron concentration was similar to the Si concentration measured by SIMS,

in the  $10^{18} \text{ cm}^{-3}$  range [85]. Several reasons have been pointed out as possible explanations for an electron density drop with the Al mole fraction: (a) deepening of the Si-donor level with the Al%; (b) formation of deep donors (DX centers); and (c) compensation by acceptors. Concerning point (a) a recent work by Katsuragawa et al. [87] shows that the Si-donor ionization energy increases with the Al mole fraction up to 20% following the hydrogenic model, but the authors show no data beyond 20% to support or deny a sharp donor deepening. The point is that the increase of the donor depth with Al%, considering a hydrogenic model, is monotonous and rather small, so that, no sharp decrease of the electron density should be expected. The transition of Si-donors to DX centers in AlGaAs layers is well documented as the deepening of the substitutional donor by a lattice relaxation process upon electron capture (strong electron–phonon coupling) [88,89]. This sharp donor deepening for Al mole fractions near the bandgap crossover in AlGaAs leads to a strong reduction of the Hall electron density, that deviates markedly from the true donor density derived either from  $C-V$  or SIMS measurements (decrease of ionization factor). This is not the case for the Si-doped AlGaN layer with 58% Al content reported by Bremser et al. [85]. Besides, theoretical predictions suggest that Si-donors do not undergo a DX transition in AlGaN [90,91]. On the other hand, oxygen, assumed for some authors to be the origin of the residual n-type conductivity in undoped AlGaN layers, was found to behave as a DX center from theoretical predictions by Stampfl et al. [90,91], and a simple experimental evidence may be given by the presence of strong persistent photoconductivity effects at low temperatures [89,89]. If this is the case, the negative-U character of the DX centers, binding two electrons at the ground state [88,89], must be considered as a further sink of free electrons in samples where, both, intentional doping and oxygen contamination coexist [85]. Compensation mechanisms may lead to a substantial reduction of the free electron density, being possible candidates carbon and/or point defects like Al and Ga vacancies acting as triple acceptors, most probable under N-rich conditions [90,91] and for Al mole fractions near 50%.

## 8. Be-doped Ga(Al)N layers on AlN buffered Si(1 1 1)

7N purity metallic Be was used for p-type doping of optimized GaN layers grown on AlN buffered Si(1 1 1), raising the temperature cell from 700°C to 910°C. Fig. 22 shows PL spectra of some Be-doped GaN layers together with a reference, undoped one. The reference sample spectrum is similar to that displayed in Fig. 19 dominated by an excitonic emission at 3.466 eV, typical of layers under tensile biaxial strain. Be-doped samples show, in addition to this excitonic emission, a peak at 3.384 eV with two-phonon replica that become more intense as the Be concentration increases. The inset in Fig. 22 shows the SIMS Be concentration increasing exponentially with the reciprocal Be-cell temperature. The emission at 3.384 eV and its phonon replica

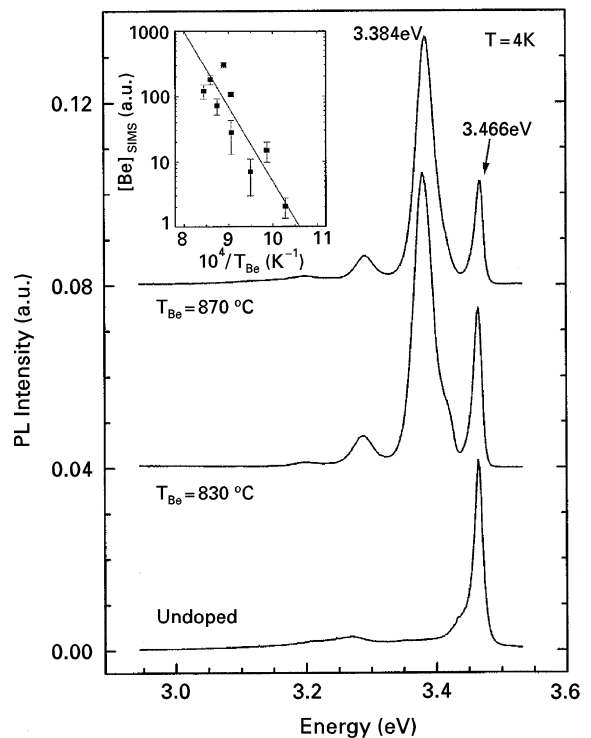


Fig. 22. Low-temperature PL spectra of GaN layers with increasing Be doping. The inset shows the Arrhenius plot of the Be concentration from SIMS as a function of the reciprocal Be-cell temperature.

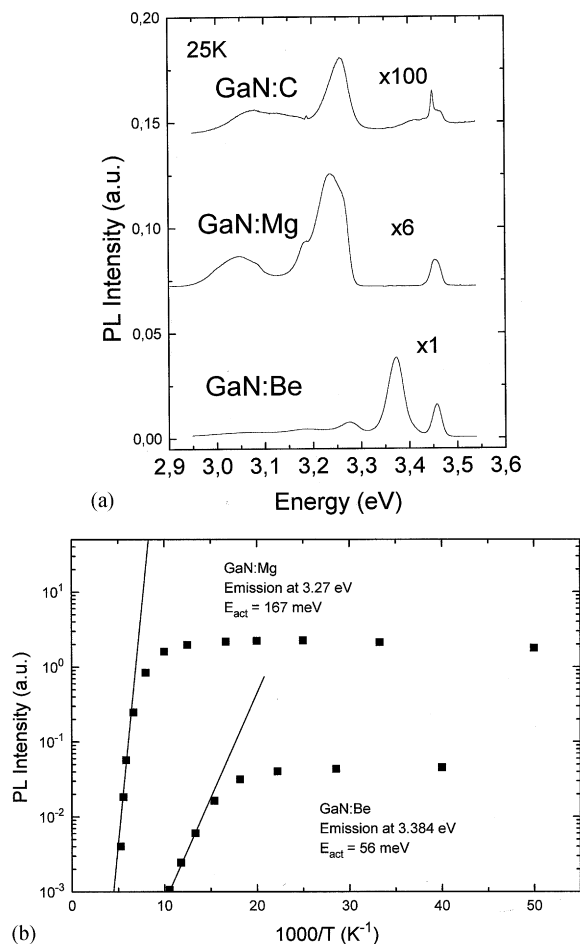


Fig. 23. (a) Low-temperature PL spectra of GaN samples doped with C, Mg, and Be. (b) Thermal quenching of the Be and Mg-related DAP transitions in GaN layers.

blueshift with increasing temperature and excitation power, and time-resolved PL spectra reveal strong non-exponential decays with very long lifetimes [92,93], all typical features of a donor–acceptor pair (DAP) recombination. A similar behavior has been already observed in Be-doped GaN layers grown by MBE on sapphire [94]. Assuming a DAP character for the emission at 3.384 eV and considering the presence of residual donors at 30–35 meV [68,69], an acceptor ionization energy around 90–100 meV is derived, which is less than half the value reported for the usual acceptors like Mg and C [95]. Fig. 23 shows PL spectra of GaN layers doped with C, Mg, and Be where the differ-

ences in acceptor energies are evident. A shallower acceptor level for Be was theoretically predicted by Bernardini et al. [96,97] at some 60 meV, in agreement with theoretical predictions of hydrogenic acceptor levels by Pödör et al. [98] and by Orton [99].

Data in Fig. 22 shows that, beyond a given Be-cell temperature, the DAP signal at 3.384 eV tends to saturate, whereas the amount of Be in the GaN layer, measured by SIMS, keeps increasing. Simultaneously, a deep PL band centered at around 2.5 eV develops (Fig. 24a) and its integrated intensity scales the Be concentration measured by SIMS (Fig. 24b). This points to a saturation of the Be incorporated as substitutional in Ga sites, while the excess Be relates to the deep band. This deep PL band was early found by Illegems and Dingle [100] in Be-doped GaN grown by vapor-phase epitaxy (VPE) on  $\text{Al}_2\text{O}_3$  and by Pankove and Hutchby [101] in Be-implanted GaN, and more recently, by Salvador et al. [102]. Bernardini et al. [96,97] suggested the formation of Be-related defects ( $\text{Be}_3\text{N}_2$ ), establishing a limit for the substitutional Be ( $\text{Be}_{\text{Ga}}$ ) around  $10^{17} \text{ cm}^{-3}$ . Neugebauer and Van de Walle [103] proposed the complex  $\text{Be}-\text{V}_{\text{N}}$  as responsible for this deep band and also pointed to the possibility of compensation by  $\text{Be}_{\text{I}}$  acting as donors, based on its lower formation energy as compared to  $\text{Be}_{\text{Ga}}$ . Bernardini et al. [96] have also proposed that the Be solubility may be enhanced by “catalysis” driven by hydrogen or oxygen. Indeed, Brand et al. [104] have reported a very high hole density ( $5 \times 10^{19} \text{ cm}^{-3}$ ) by codoping with Be–O in  $\beta$ -GaN grown on GaAs, although, to our knowledge, these results were not confirmed by other researchers. Being Be the shallowest acceptor in GaN the point is how to increase its solubility, either by codoping or through techniques trying to avoid the complex defect formation, but, so far, there is no clear evidence about the actual chemical structure of such defects.

Hall measurements in Be-doped GaN layers, grown on top of thick (1  $\mu\text{m}$ ) AlGaIn buffers to avoid the parallel conduction at the interface due to interdiffusion, revealed a highly resistive behavior, but not a true p-type conductivity. Considering the n-type residual concentration around  $2 \times 10^{17} \text{ cm}^{-3}$  and assuming the Be solubility limit

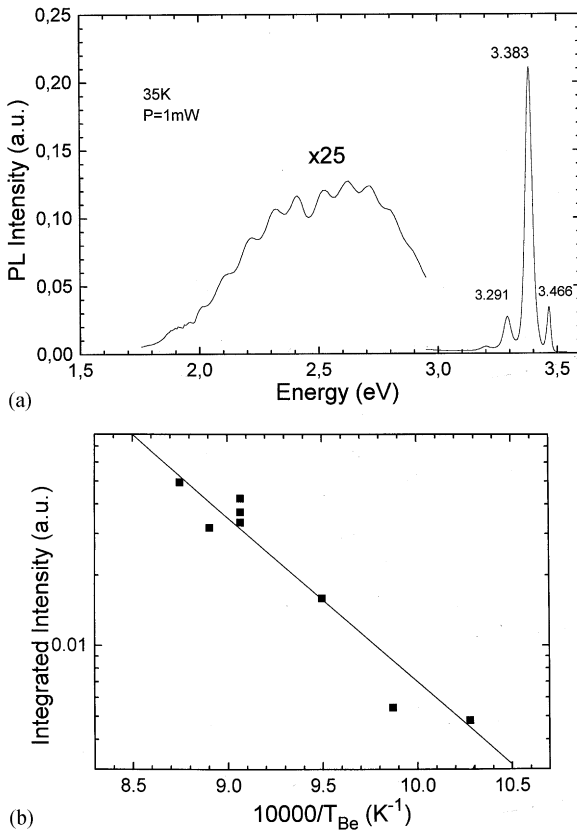


Fig. 24. (a) Low-temperature PL spectrum of a GaN sample doped with Be. (b) Integrated intensity of the emission centered around 2.5 eV in (a) as a function of the Be cell temperature.

calculated by Bernardini et al. [96,97], about  $10^{17} \text{ cm}^{-3}$ , it seems reasonable to get semi-insulating layers. Mg-doping, although generating deeper acceptor levels, presents a higher solubility in GaN, leading to layers with a clear p-type conductivity. Mg-doped GaN layers grown on Si(1 1 1) reveal p-type conductivity, and a Mg:GaN/Si:AlGaN LED heterostructure exhibits a blue-green emission at room temperature.

## 9. Summary

A review of the growth optimization, doping effects, and transport and optical properties of wurtzite Ga(Al)N layers grown on Si(1 1 1) by plasma-assisted MBE is given. High crystal quality is

achieved in GaN and AlGaIn layers, with fingerprints, like XRD-FWHM values, surface roughness, residual n-type conductivity ( $2 \times 10^{17} \text{ cm}^{-3}$ ), and excitonic PL emissions comparable to most Ga(Al)N layers grown by MBE on substrates like sapphire and 6H-SiC. A strong and reproducible change in crystal morphology is observed as a function of the III/V ratio, leading to columnar, compact, or mixed layers. Optimized, compact Ga(Al)N layers are grown under III/V ratios close to stoichiometry, these layers being under a biaxial tensile strain of thermal origin. GaN layers doped with Si exhibit very high electron densities ( $2 \times 10^{19} \text{ cm}^{-3}$ ), and the role of Si-doping in the growth mode leading to a significant dislocation density reduction, by a factor of 10, has been established. The Si-donor ionization energy derived from PL and temperature-dependent Hall data, around 50–60 meV, is significantly higher than most values reported in the literature. Si-doped AlGaIn layers (with  $x < 0.4$ ) reach very high electron densities ( $8 \times 10^{19} \text{ cm}^{-3}$ ), but the doping efficiency drops for Al% fractions higher than 40%. The origin of this efficiency decrease, being similar to that observed in MOVPE-grown AlGaIn/Al<sub>2</sub>O<sub>3</sub>, is still unknown. Substitutional Be in GaN generates the shallowest acceptor known to date (90–100 meV), but its solubility substituting Ga atoms is rather small, as compared to that of Mg. Further works aiming to increase this solubility, by codoping or by  $\delta$ -doping or low-temperature doping, are underway.

## Acknowledgements

The authors wish to acknowledge the financial support provided by CICYT Projects TIC95-0770, MAT98-0823-C03-01, and MAT98-0823-C03-02, by EU ESPRIT LTR Project 20968 (Laquani), and Junta de Andalucía (Group PAI TEP 0120).

## References

- [1] S. Nakamura, M. Senoh, S.I. Nagahama, N. Iwasa, T. Yamada, T. Matsushita, H. Kiyoku, Y. Sugimoto, T. Kozaki, H. Umemoto, M. Sano, K. Chocho, Appl. Phys. Lett. 72 (1998) 2014.

- [2] A. Ohtani, K.S. Stevens, R. Beresford, *Appl. Phys. Lett.* 65 (1994) 61.
- [3] A. Bourret, A. Barski, J.L. Rouvière, G. Renaud, A. Barbier, *J. Appl. Phys.* 83 (1998) 2003.
- [4] M.A. Sánchez-García, E. Calleja, E. Monroy, F.J. Sánchez, F. Calle, E. Muñoz, R. Beresford, *J. Crystal Growth* 183 (1998) 23.
- [5] M. Godlewski, J.P. Bergman, B. Monemar, U. Rossner, A. Barski, *Appl. Phys. Lett.* 69 (1996) 2089.
- [6] K.S. Stevens, M. Kinniburgh, A.F. Schwartzman, A. Ohtani, R. Beresford, *Appl. Phys. Lett.* 66 (1995) 3179.
- [7] A. Osinsky, S. Gangopadhyay, J.W. Yang, R. Gaska, D. Kuksenkov, H. Temkin, I.K. Shmagin, Y.C. Chang, J.F. Muth, R.M. Kolbas, *Appl. Phys. Lett.* 72 (1998) 551.
- [8] S. Guha, N.A. Bojarczuk, *Appl. Phys. Lett.* 72 (1998) 415.
- [9] K.S. Stevens, A. Ohtani, M. Kinniburgh, R. Beresford, *Appl. Phys. Lett.* 65 (1994) 321.
- [10] M.A. Sánchez-García, E. Calleja, F.J. Sánchez, F. Calle, E. Monroy, D. Basak, E. Muñoz, C. Villar, A. Sáenz-Hervás, M. Aguilar, J.J. Serrano, J.M. Blanco, *J. Electron. Mater.* 27 (1998) 276.
- [11] H.J. Wen, M. Dähne-Prietsch, A. Bauer, M.T. Cuberes, I. Manke, G. Kaindl, *J. Vac. Sci. Technol. A* 13 (1995) 2399.
- [12] B.N. Sverdlov, G.A. Martin, H. Morkoç, D.J. Smith, *Appl. Phys. Lett.* 67 (1995) 2063.
- [13] S. Tanaka, R. Scott Kern, R.F. Davis, *Appl. Phys. Lett.* 66 (1995) 37.
- [14] L.T. Romano, J.E. Northrup, M.A. O'Keefe, *Appl. Phys. Lett.* 69 (1996) 2394.
- [15] X.H. Wu, P. Fini, S. Keller, E.J. Tarsa, B. Heying, U.K. Mishra, S.P. DenBaars, J.S. Speck, *Jpn. J. Appl. Phys.* 35 (1996) L1648.
- [16] U. Strauss, H. Tews, H. Riechert, R. Averbeck, M. Schienle, B. Jobst, D. Volm, T. Streibl, B.K. Meyer, W.W. Rühle, *Semicond. Sci. Technol.* 12 (1997) 637.
- [17] T.D. Moustakas, T. Lei, R.J. Molnar, *Physica B* 185 (1993) 36.
- [18] T. Lei, K.F. Ludwig, T.D. Moustakas, *J. Appl. Phys.* 74 (1993) 4430.
- [19] K. Dovidenko, S. Oktyabrsky, J. Narayan, M. Razeghi, *J. Appl. Phys. Lett.* 79 (1996) 2439.
- [20] E. Calleja, M.A. Sánchez-García, E. Monroy, F.J. Sánchez, E. Muñoz, A. Sáenz-Hervás, C. Villar, M. Aguilar, *J. Appl. Phys.* 82 (1997) 4681.
- [21] M. Miyauchi, Y. Ishikawa, N. Shibata, *Jpn. J. Appl. Phys.* 31 (1992) L1714.
- [22] W.J. Meng, T.A. Perry, *J. Appl. Phys.* 76 (1994) 7824.
- [23] K. Yasutake, A. Takeuchi, H. Kakiuchi, K. Yoshii, *J. Vac. Sci. Technol. A* 16 (1998) 2140.
- [24] S. Guha, N.A. Bojarczuk, D.W. Kisker, *Appl. Phys. Lett.* 69 (1996) 2879.
- [25] R.C. Powell, N.E. Lee, Y.W. Kim, J.E. Greene, *J. Appl. Phys.* 73 (1993) 189.
- [26] Z. Yu, S.L. Buczkowski, N.C. Giles, T.H. Myers, M.R. Richards-Babb, *Appl. Phys. Lett.* 69 (1996) 2731.
- [27] M. Yoshizawa, A. Kikuchi, M. Mori, N. Fujita, K. Kishino, *Jpn. J. Appl. Phys.* 36 (1997) L459.
- [28] I. Akasaki, H. Amano, H. Murakami, M. Sassa, H. Kato, K. Manabe, *J. Crystal Growth* 128 (1993) 379.
- [29] T. Zywiets, J. Neugebauer, M. Scheffler, *Appl. Phys. Lett.* 73 (1998) 487.
- [30] D.K. Gaskill, N. Bottka, M.C. Lin, *Appl. Phys. Lett.* 48 (1986) 1449.
- [31] F. Calle, F.J. Sánchez, J.M.G. Tijero, M.A. Sánchez-García, E. Calleja, R. Beresford, *Semicond. Sci. Technol.* 12 (1997) 1396.
- [32] M.A. Sánchez-García, E. Calleja, F.B. Naranjo, F.J. Sánchez, F. Calle, E. Muñoz, A.M. Sánchez, F.J. Pacheco, S.I. Molina, *J. Crystal Growth* 201/202 (1999) 415.
- [33] E. Calleja, M.A. Sánchez-García, D. Basak, F.J. Sánchez, F. Calle, P. Youinou, E. Muñoz, J.J. Serrano, J.M. Blanco, C. Villar, T. Laine, J. Oila, K. Saarinen, P. Hauttojarvi, C.H. Molloy, D.J. Sommerford, I. Harrison, *Phys. Rev. B* 58 (1998) 1550.
- [34] P. Kung, A. Saxler, X. Zhang, D. Walker, T.C. Wang, I. Ferguson, M. Razeghi, *Appl. Phys. Lett.* 66 (1995) 2958.
- [35] E.S. Hellman, D.N.E. Buchanan, C.H. Chen, *MRS Internet J. Nitride Semicond. Res.* 3 (1998) 43.
- [36] J.F. Valtueña, A. Sacedón, A.L. Alvarez, I. Izpura, F. Calle, E. Calleja, G. MacPherson, P.J. Goodhew, F.J. Pacheco, R. García, S.I. Molina, *J. Crystal Growth* 182 (1997) 281.
- [37] A.R. Smith, V. Ramachandran, R.M. Feenstra, D.W. Greve, M.S. Shin, M. Sowronski, J. Neugebauer, J.E. Northrup, *J. Vac. Sci. Technol. A* 16 (1998) 1641.
- [38] A very good and thorough review is given by E.S. Hellman, *MRS Internet J. Nitride Semicond. Res.* 3 (1998) 11.
- [39] Z. Yang, F. Guarin, I.W. Tao, W.I. Wang, S.S. Iyer, *J. Vac. Sci. Technol. B* 13 (1995) 789.
- [40] A.J. Steckl, J. Devrajan, C. Tran, R.A. Stall, *Appl. Phys. Lett.* 69 (1996) 2264.
- [41] J.W. Yang, C.J. Sun, Q. Chen, M.Z. Anwar, M. Asif-Kahn, S.A. Nikishin, G.A. Seryogin, A.V. Osinsky, L. Chernyak, H. Temkin, C. Hu, S. Mahajant, *Appl. Phys. Lett.* 69 (1996) 3566.
- [42] L. Wang, X. Liu, Y. Zan, J. Wang, D. Wang, D.C. Lu, Z. Wang, *Appl. Phys. Lett.* 72 (1998) 109.
- [43] N.P. Kobayashi, J.T. Kobayashi, P.D. Dapkus, W.J. Choi, E. Bond, X. Zhang, D.H. Rich, *Appl. Phys. Lett.* 71 (1997) 3569.
- [44] D. Brunner, H. Angerer, E. Bustarret, F. Freudenberg, R. Höpler, R. Dimitrov, O. Ambacher, M. Stutzmann, *J. Appl. Phys.* 82 (1997) 5090.
- [45] H. Angerer, D. Brunner, F. Freudenberg, O. Ambacher, M. Stutzmann, R. Höpler, T. Metzger, E. Born, G. Dollinger, A. Bergmaier, S. Karsch, H.J. Körner, *Appl. Phys. Lett.* 71 (1997) 1504.
- [46] D.K. Wickenden, C.B. Barger, W.A. Bryden, J. Miragliotta, T.J. Kistenmacher, *Appl. Phys. Lett.* 65 (1994) 2024.
- [47] M.A. Kahn, R.A. Skogman, R.G. Schulze, M. Gershenson, *Appl. Phys. Lett.* 43 (1983) 492.
- [48] S. Yoshida, S. Misawa, S. Gonda, *J. Appl. Phys.* 53 (1982) 6844.

- [49] Y. Koide, H. Itoh, M.R.H. Kahn, K. Hiramatsu, N. Sawaki, I. Akasaki, *J. Appl. Phys.* 61 (1987) 4540.
- [50] M.R.H. Kahn, Y. Koide, H. Itoh, N. Sawaki, I. Akasaki, *Sol. State Commun.* 60 (1986) 509.
- [51] M.D. Bremser, W.G. Perry, T. Zheleva, N.V. Edwards, O.H. Nam, N. Parikh, D.E. Aspnes, R.F. Davis, *Mater. Res. Soc. Internet J. Nitrides Semicond. Res.* 1 (1996) 8.
- [52] T.F. Huang, J.S. Harris, *Appl. Phys. Lett.* 72 (1998) 1158.
- [53] D. Korakakis, H.M. Ng, M. Misra, W. Grieshaber, T.D. Moustakas, *Mater. Res. Soc. Internet J. Nitrides Semicond. Res.* 1 (1996) 10.
- [54] T. Takeuchi, H. Takeuchi, S. Sota, H. Sakai, H. Amano, I. Akasaki, *Jpn. J. Appl. Phys.* 36 (1997) L177.
- [55] E. Calleja, F.J. Sánchez, M.A. Sánchez-García, F. Calle, F.B. Naranjo, E. Muñoz, S.I. Molina, R. García, unpublished.
- [56] L.K. Li, J. Alperin, W.I. Wang, D.C. Look, D.C. Reynolds, *J. Vac. Sci. Technol. B* 16 (1998) 1275.
- [57] D.C. Look, D.C. Reynolds, W. Kim, O. Aktas, A. Botchkarev, A. Salvador, H. Morkoç, *J. Appl. Phys.* 80 (1996) 2960.
- [58] R.J. Molnar, T. Lei, T.D. Moustakas, *Appl. Phys. Lett.* 62 (1993) 72.
- [59] D.L. Rode, D.K. Gaskill, *Appl. Phys. Lett.* 66 (1995) 1972.
- [60] L.B. Rowland, K. Doverspike, D.K. Gaskill, *Appl. Phys. Lett.* 66 (1995) 1495.
- [61] D.K. Gaskill, A.E. Wickenden, K. Doverspike, B. Tadayon, L.B. Rowland, *J. Electron. Mater.* 24 (1995) 1525.
- [62] H.M. Ng, D. Doppalapudi, T.D. Moustakas, N.G. Weimann, L.F. Eastman, *Appl. Phys. Lett.* 73 (1998) 821.
- [63] N.G. Weimann, L.F. Eastman, D. Doppalapudi, H.M. Ng, T.D. Moustakas, *J. Appl. Phys.* 83 (1998) 3656.
- [64] H.Y. Fan, *Phys. Rev.* 82 (1951) 900.
- [65] M. Leszczynski, H. Teisseyre, T. Suski, I. Grzegory, M. Bockowski, J. Jun, S. Porowski, K. Pakula, J.M. Baranowski, C.T. Foxon, T.S. Cheng, *Appl. Phys. Lett.* 69 (1996) 73.
- [66] A. Shikanai, T. Azuhata, T. Sota, S. Chichibu, A. Kuramata, K. Horino, S. Nakamura, *J. Appl. Phys.* 81 (1997) 417.
- [67] W.G. Perry, T. Zheleva, M.D. Bremser, R.F. Davis, W. Shan, J.J. Song, *J. Electron. Mater.* 26 (1997) 224.
- [68] D. Volm, K. Oettinger, T. Streibl, D. Kovalev, M. Ben-Chorin, J. Diener, B.K. Meyer, J. Majewski, L. Eckey, A. Hoffmann, H. Amano, I. Akasaki, K. Hiramatsu, D.T. Detchprohm, *Phys. Rev. B* 53 (1996) 16543.
- [69] C. Merz, M. Kunzer, U. Kaufmann, *Semicond. Sci. Technol.* 11 (1996) 712.
- [70] D. Kovalev, B. Averboukh, D. Volm, B.K. Meyer, H. Amano, I. Akasaki, *Phys. Rev. B* 54 (1996) 2518.
- [71] E. Oh, H. Park, Y. Park, *Appl. Phys. Lett.* 72 (1998) 1848.
- [72] E.F. Schubert, I.D. Goepfert, W. Grieshaber, J.M. Redwing, *Appl. Phys. Lett.* 71 (1997) 921.
- [73] E. Lliopoulos, D. Doppalapudi, H.M. Ng, T.D. Moustakas, *Appl. Phys. Lett.* 73 (1998) 375.
- [74] I.-H. Lee, I.-H. Choi, C.R. Lee, S.K. Noh, *Appl. Phys. Lett.* 71 (1997) 1359.
- [75] S. Ruvimov, Z. Liliental-Weber, T. Suski, J.W. Ager III, J. Washburn, J. Krueger, C. Kisielowski, E.R. Weber, H. Amano, I. Akasaki, *Appl. Phys. Lett.* 69 (1996) 990.
- [76] X. Zhang, Soo-Jin Chua, W. Liu, K.-B. Chong, *Appl. Phys. Lett.* 72 (1998) 1890.
- [77] O. Langerstedt, B. Monemar, *Phys. Rev. B* 19 (1979) 3064.
- [78] C. Kisielowski, J. Krüger, S. Ruvimov, T. Suski, J.W. Ager III, E. Jones, Z. Liliental-Weber, M. Rubin, E.R. Weber, M.D. Bremser, R.F. Davis, *Phys. Rev. B* 54 (1996) 17745.
- [79] M. Leszczynski, P. Prystawko, A. Sliwinski, H. Teisseyre, T. Suski, M. Bockowski, S. Porowski, R. Paszkiewicz, M. Tlaczala, B. Beaumont, P. Gibart, A. Barski, R. Langer, M. Kamp, C. Kirchner, *MRS Internet J. Nitride Semicond. Research*, in press.
- [80] S.I. Molina, A.M. Sánchez, F.J. Pacheco, R. García, M.A. Sánchez-García, E. Calleja, unpublished.
- [81] J.R. Haynes, *Phys. Rev. Lett.* 4 (1960) 361.
- [82] A.E. Wickenden, L.B. Rowland, K. Doverspike, D.K. Gaskill, J.A. Freitas, D.S. Simons, P.H. Chi, *J. Electron. Mater.* 24 (1995) 1547.
- [83] Y. Kawakami, Z.G. Peng, Y. Narukawa, S. Fujita, S. Fujita, S. Nakamura, *Appl. Phys. Lett.* 69 (1996) 1414.
- [84] J.W. Orton, S. Sakai, *MRS Internet J. Nitride Semicond. Research*, in press.
- [85] M.D. Bremser, W.G. Perry, O.H. Nam, D.P. Griffis, R. Loesing, D.A. Ricks, R.F. Davis, *J. Electron. Mater.* 27 (1998) 229.
- [86] H.G. Lee, M. Gershenzon, B.L. Goldenberg, *J. Electron. Mater.* 20 (1991) 621.
- [87] M. Katsuragawa, S. Sota, M. Komori, C. Anbe, T. Takeuchi, H. Sakai, H. Amano, I. Akasaki, *J. Crystal Growth* 189/190 (1998) 528.
- [88] Good reviews on this topic are: P.M. Mooney, *J. Appl. Phys.* 67 (1990) R1.
- [89] P.M. Mooney, DX Centers-donors in AlGaAs and related compounds, in: E. Muñoz (Ed.), *Defect and Diffusion Forum*, vol. 108, 1994, Scitec Publications, Switzerland.
- [90] C. Stampfl, C.G. Van de Walle, *Appl. Phys. Lett.* 72 (1998) 459, and references therein.
- [91] W.G. Perry, M.B. Bremser, R.F. Davis, *J. Appl. Phys.* 83 (1998) 469.
- [92] F.J. Sánchez, F. Calle, M.A. Sánchez-García, E. Calleja, E. Muñoz, C.H. Molloy, D.J. Somerford, J.J. Serrano, J.M. Blanco, *Semicond. Sci. Technol.* 13 (1998) 1130.
- [93] F.J. Sánchez, F. Calle, M.A. Sánchez-García, E. Calleja, E. Muñoz, C.H. Molloy, D.J. Somerford, F.K. Koschnick, K. Michael, M.J. Spaeth, *MRS Internet J. Nitride Semicond. Res.* 3 (1998) 19.
- [94] D.J. Dewsnap, A.V. Andrianov, I. Harrison, J.W. Orton, D.E. Lacklison, G.B. Ren, S.E. Hooper, T.S. Cheng, C.T. Foxon, *Semicond. Sci. Technol.* 13 (1998) 500.
- [95] S. Fisher, C. Wetzel, E.E. Haller, B.K. Meyer, *Appl. Phys. Lett.* 67 (1995) 1298.

- [96] F. Bernardini, V. Fiorentini, A. Bosin, *Appl. Phys. Lett.* 70 (1997) 2990.
- [97] J. Neugebauer, C.G. Van de Walle, *Appl. Phys. Lett.* 68 (1996) 1829.
- [98] B. Pödör, *Semicond. Sci. Technol.* 11 (1996) 827.
- [99] J.W. Orton, *Semicond. Sci. Technol.* 10 (1995) 101.
- [100] M. Ilegems, R. Dingle, *J. Appl. Phys.* 44 (1973) 4234.
- [101] J.I. Pankove, J.A. Hutchby, *J. Appl. Phys.* 47 (1976) 5387.
- [102] A. Salvador, W. Kim, Ö. Aktas, A. Botchkarev, H. Morcoç, *Appl. Phys. Lett.* 69 (1996) 2692.
- [103] J. Neugebauer, C.G. Van de Walle, *MRS Internet J. Nitride Semicond. Res.*, in press.
- [104] O. Brandt, H. Yang, H. Kostial, K.H. Ploog, *Appl. Phys. Lett.* 69 (1996) 2707.